geoconvention
Calgary • Canada • May 12-14 2025

Coupled Reservoir-Geomechanics Study of CO_2 Injection Effects on Seal Integrity and Fault Stability in a Suboptimal Depleted Oil Reservoir of the Hugin Formation, Volve Field, North Sea

Ahmad Brahmanta Aulia, Elena Konstantinovskaya
Department of Earth and Atmospheric Sciences, University of Alberta

Summary

Carbon capture and sequestration (CCS) is a crucial tool to abate carbon emission and mitigate the adverse effect of climate change. Compared to other geological alternatives, converting depleted hydrocarbon reservoirs into CCS sites offer several practical advantages, including their known geological characteristics, proven storage integrity, pre-existing facilities, and prevalent regional availability. Nevertheless, safely and reliably converting depleted reservoirs into a CCS site is not without challenges. Previous research finds that out of 1,317 depleted oil and gas fields in the Gulf of Mexico, only 31 fields are suitable for carbon storage when assessed with standard site screening and risk assessment criteria (Callas et al., 2022). Additionally, multiple studies establish that reservoir depletion due to hydrocarbon production can cause subsurface stress perturbation, leading to stress rotation, poroelastic deformation in the reservoir interval and caprock, and fault reactivation, further complicating optimal CO_2 injection scenario in order to minimize risks (Zoback, 2007).

In this research, we evaluated the feasibility and safety of converting a suboptimal depleted hydrocarbon reservoir at the Volve oil field in the North Sea into a CCS site. To achieve the stated purpose, we implemented a comprehensive workflow, integrating 3D geological modeling, 1D-3D mechanical earth modeling (MEM), reservoir simulations, and one way coupled reservoir-geomechanical modeling. We employed these methods to address key objectives: (1) estimating the total potential CO_2 injection volume, (2) determining critical injection pressures to avoid hydraulic fracturing in the reservoir and caprock, (3) examining interactions between injected CO_2 and residual oil in the reservoir, and (4) assessing the potential for fault shear-slip reactivation during reservoir repressurization.

Geological Background and Depletion History of Volve Field

The Volve Field is a depleted offshore oil field located in Block 15/9 in the Southern Norwegian North Sea, situated around 200 km west of Stavanger and 5 km north of Sleipner East Field at a water depth of around 80 – 100 m (Fig.1).

Hydrocarbon accumulation is found within a fault-bounded domal structure that covers an area of 2 km by 3 km in size, formed by the collapse of Zechstein Salt Formation affecting the overlying Jurassic and Triassic layers (Szydlik et al., 2006; Karlo et al., 2014). The primary oil reservoir of the field is the Jurassic sandstone of the Hugin Formation, consisting of fine to medium-grained marine sandstones with moderate cementation. Hugin Formation at the Volve Field exhibits excellent reservoir properties and average thickness of 10-30 m. The reservoir is overlain by the Draupne Formation serving as both the regional seal and source rock, with thickness varying from

a few meters at the dome crest to several hundred meters along the flanks. Underlying the Hugin Formation is the Sleipner Formation, which consist of wet sandstone interbedded with thin breaks of claystone and coal (NPD, 1984).

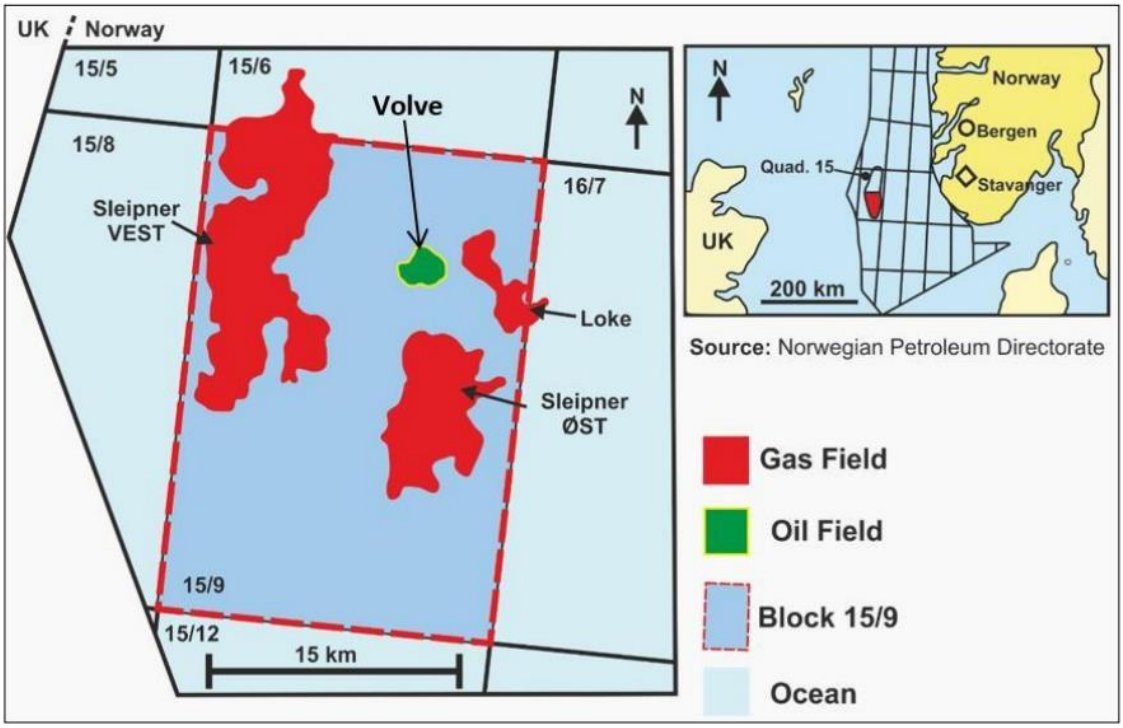

Fig. 1. Location of the Volve Field within the 15/9 block. Volve Field is a depleted oil field surrounded by gas fields including Sleipner West, Sleipner East, and Loke Fields (from Ravasi et al., 2015).

The sedimentary succession of the Norwegian North Sea Basin is characterized by a normal faulting stress regime, with the maximum horizontal stress (SH_{max}) predominantly oriented NW-SE (Fig. 2). Closer to the Volve Field however, SH_{max} seem to rotate clockwise to N115^{o} (Grollimund et al., 2001). The variation in SH_{max} orientation within the sedimentary layers, which are detached from the basement in the Central North Sea, may be influenced by the presence of Zechstein Salt (Hillis and Nelson, 2005).

The Volve Field was discovered in 1993 and hydrocarbon production began in 2008 from sandstone of Middle Jurassic age in the Hugin Formation. The reservoir is at a depth of 2800-3100 meters (Norwegian Offshore Directorate, 2025). The estimated original oil in place is approximately 140 million barrels. Initially, the reservoir pressure was around 33 MPa, which was the primary driver of oil production. However, the reservoir pressure quickly declined to approximately 27.5–29 MPa, and within a year of production, enhanced recovery techniques such as water injection was implemented to maintain output. The maximum annual production was achieved in 2009 consisting of (in Million Sm^3 oil equivalents): 2.72 oil, 0.3 gas, 0.12 natural gas liquids (NGL), and 0.04 condensate. Production peaked at 56,000 barrels per day but steadily declined thereafter (Fig. 3). By 2016, the field was abandoned after producing about 63 million

barrels, marking the end of its economically viable operation. Notably, it is estimated that 40% of the oil remained in the reservoir at the time of abandonment (Equinor, 2018; Weijermars, 2024).

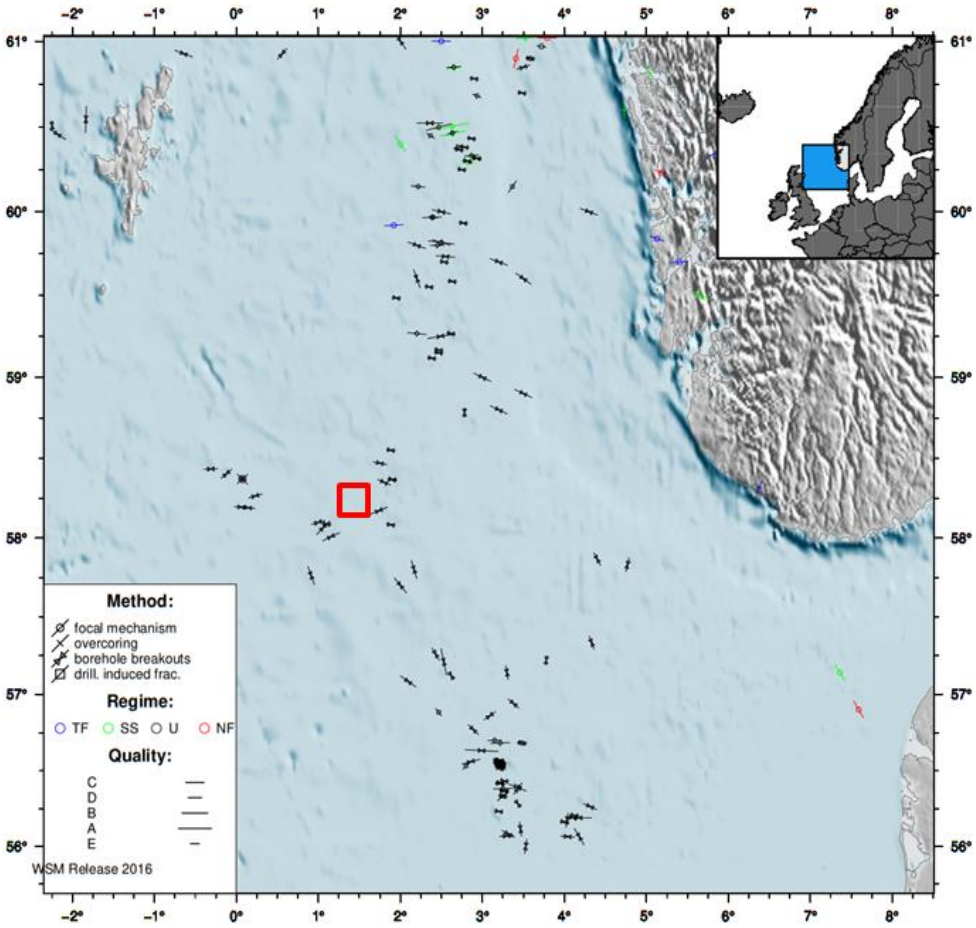

Fig. 2. SH_{max} in the Norwegian North Sea is primarily oriented E-W. South of 59°, this orientation rotated clockwise to around 115° (Grollimund et al., 2001; Heidbach et al., 2018). The location of the Volve Field is indicated by the red box.

Data and Methods

To complete this study, we utilize the open-source dataset of the depleted Volve Field, made available by Equinor (Equinor, 2018). This dataset consist of a comprehensive collection of information, including 3D seismic amplitude data in both time and depth domains, interpreted horizons and faults, reservoir pressure and saturation data throughout the production lifecycle, well drilling and production data (covering both producers and injectors), petrophysical and geomechanical testing data, well testing data, LOT data, and detailed well reports.

We conducted a petrophysical analysis in Techlog™ to evaluate the reservoir properties of the Hugin Formation and determine the most suitable injection intervals, utilizing well logs and core measurement data from exploration wells 15/9-19 A, 15/9-19 BT2, and 15/9-19 SR. We estimated

the shale volume along the wellbore using linear relationship of the gamma ray log. Next, we calculated the total porosity using density logs and formation density data referenced in literature. We calibrated the calculated total porosity against depth-corrected core measurements for accuracy. Then, we derived total porosity-permeability relationship based on core petrophysical measurements within the cored interval and used it to estimate the permeability along the length of the wellbore.

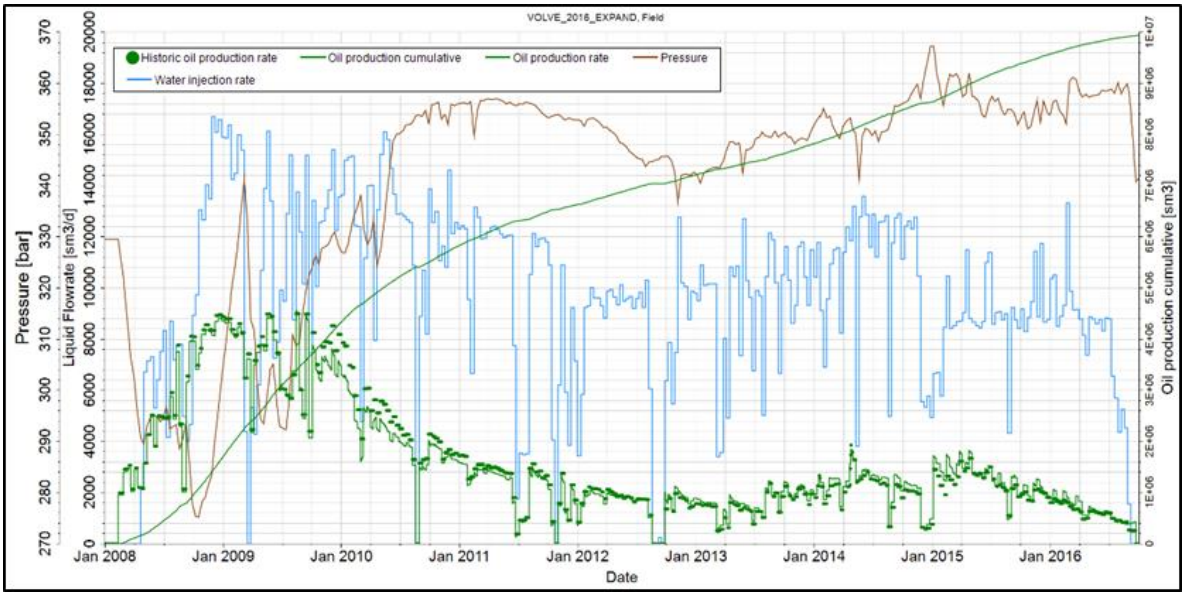

Fig. 3. Historic production profile of the Volve Field based on original data by Equinor (2018). Reservoir pressure declined quickly within the first year of production. Water injection was implemented to maintain production, which inadvertently increase the reservoir pressure to around 36 MPa by the time production ceased.

We built a 3D geological model of the Volve Field in Petrel™ based on pre-existing geological model available in the open-source data in combination with additional geophysical interpretations that we conducted using the 3D amplitude seismic volume in depth domain of the study area that was acquired in 2010. The resulting geological model integrates 18 seismic horizons and 36 faults in total, consisting of 6.5 million cells with a resolution of 50 x 50 m, and an average cell thickness of 7.5 m (0.97 m within the Hugin Formation interval). We then populated the 3D geological model with petrophysical and geomechanical properties from petrophysical analysis and 1D MEM modeling results, respectively.

We performed a fault seal analysis to evaluate the ability of faults to contain injected CO_2 within the Hugin Formation. We used the modeled 3D shale volume (V_{Shale}) to calculate the Shale Gouge Ratio (SGR) along the fault surfaces. We then utilized the global empirical relationship established by Yielding et al. (2010) to derive the across fault pressure difference (AFPD) and maximum CO_2 column height (h_{max}) based on the calculated SGR values. To determine the appropriate empirical relationship, it is essential to determine both the CO_2 phase density under reservoir conditions and reservoir maximum burial depth. We used a CO_2 phase density of 660 kg/m³, corresponding to a reservoir depth of approximately 2800 m, based on a North Sea geothermal gradient of 30°C/km (Bachu, 2003; Marin et al., 2022). The maximum burial depth of the Hugin Formation

was set at 3400 m, using data from the adjacent Sleipner West Field (Halland et al., 2024). We also calculated the fault transmissibility multipliers for reservoir simulation purposes using the 3D permeability property and predicted fault thickness.

We performed an initial estimation of the potential CO_2 storage capacity range within the reservoir block using Monte Carlo simulation method with 50,000 realization in RoseRA™ software. Initially, we calculated the gross rock volume (GRV) of the target reservoir in the Hugin Formation using the area versus depth method. Next, we estimated the pore volume (PV) by multiplying the GRV with the range of porosity values obtained from core data collected from exploration wells. Once the PV was calculated, we considered factors such as storage efficiency, CO_2 phase density variations within the reservoir interval, residual oil saturation, and other relevant parameters to determine the amount of CO_2 that can be stored in residual oil, brine, and pore space components within the injection target reservoir.

In this section, we outline the parameters for the Monte Carlo simulation used to estimate the CO_2 injection capacity, with all parameters displayed in P10-P90 range. We used a porosity range of 20% to 26% and a net-to-gross ratio of 70% to 90%, both derived from core petrophysical analysis of the Hugin Formation's cored interval. The oil saturation at the start of CO_2 injection was based on a dynamic reservoir model of the depleted stage, available in the dataset, with values ranging from 15% to 40%. We assumed that the injected CO_2 column would occupy 90% of the closure in the Hugin Reservoir interval (~225 m), as storing more CO_2 could increase the risk of leakage from the trap.The CO_2 density in reservoir conditions was estimated based on Bachu (2003), with a range of 660 to 700 kg/m³. Due to limited site-specific data, we also consulted existing literature for additional parameters to accurately estimate the injection capacity range. A volumetric and displacement efficiency range of 16% to 39% was used, which is applicable to storage in formations with residual oil, as referenced by IEA-GHG (2009) and Goodman et al. (2011, 2016) in Sanguinito et al. (2020). According to IEA-GHG (2009), the proportion of pore space filled with reservoir fluids that can be displaced by injected CO_2 (S_{CO2}) ranges from 0.35 to 0.76 in clastic saline aquifers. However, we applied a lower S_{CO2} range of 0.28 to 0.61 (approximately 20% lower) in our case, considering that a significant portion of the pore space remains occupied by residual oil, some of which may be immovable. We used experimental data from Mao et al. (2013) and Barclay and Mishra (2016) to estimate the final CO_2 concentration that can be stored in reservoir fluids. The values ranged from 39.6 kg/m³ to 48.4 kg/m³ for brine, and from 679 kg/m³ to 741 kg/m³ for oil. However, it's important to note that the solubility of CO2 in oil under reservoir conditions is likely much lower than the experimental values reported in these studies (Sanguinito et al., 2020).

Next, we performed 1D MEM modeling in Techlog™ on the exploration wells to analyze the magnitude of pore pressure, the in-situ total principal stresses, and derive geomechanical rock properties, such as unconfined compressive strength, Young's Modulus, Poisson's ratio, angle of internal friction, and tensile strength for the full length of the wellbore. We obtained the pore pressure profile along the wellbore using modified Eaton method (Eaton, 1975). We then calibrated the pore pressure results with the historical drilling mud weight and well testing data. We estimated the magnitude of horizontal stresses using the poroelastic horizontal strain model (Thiercelin and Plumb, 1994). Finally, we validated the resulting 1D MEM at well 15/9-19 A by conducting wellbore stability analysis and comparing the predicted borehole failures with the recorded well drilling events and borehole breakouts.

We used the 3D geological model to simulate different CO_2 injection scenarios and optimize injection volumes using Intersect™. The reservoir simulations incorporated 8 vertical injection wells positioned along the northern and southern borders of the domal structure, with different scenario of group injection rate limits (Fig. 4). To ensure reservoir and seal integrity, the maximum bottom hole pressure (BHP) of injection wells was set at 90% of the lowest calculated minimum horizontal stress (Sh_{min}) within the Draupne Shale caprock interval above the Hugin Formation. This pressure threshold is crucial for ensuring containment and preventing fracturing of the Draupne Seal layer. To analyze changes over time, we extracted reservoir pressure and saturation data from the dataset 3D reservoir model corresponding to the end of production in 2016. The oil-water contact in the reservoir model is slightly inclined to the ESE, being at about 2900 m bsl in the WNW and 3200 m bsl in the ESE (Fig. 4).

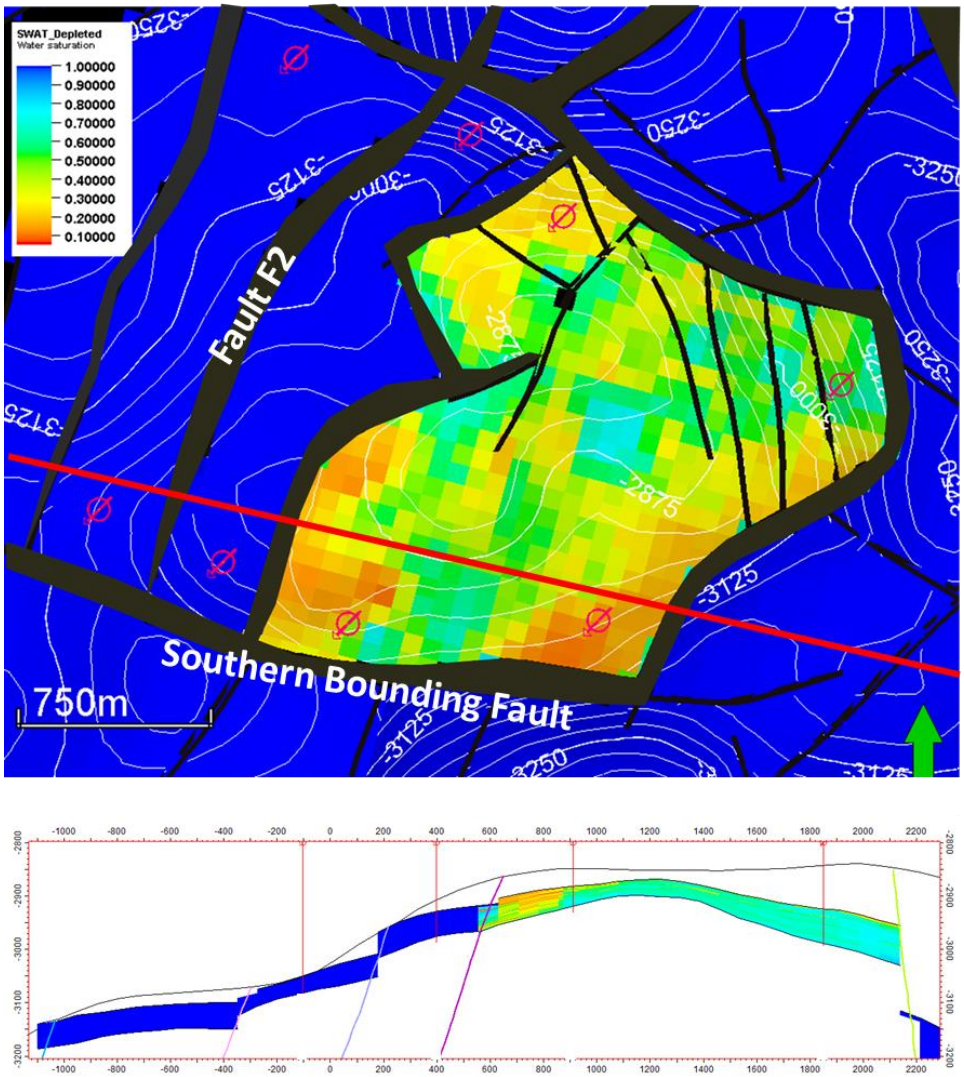

Fig. 4. Map (a) and cross-section (b) of water saturation model of the Hugin Formation after depletion (2016). The reservoir structure contour map are shown for the top of the Hugin Formation. Eight vertical CO_2 injection wells (highlighted by red circles) are placed at the flanks of the structural high (domal structure) for dynamic reservoir simulation.

Finally, we obtained the pressure buildup model from the reservoir simulation result to carry out 3D one-way coupled geomechanical simulations in Visage™ and Intersect™ to evaluate the impact of pore pressure increase caused by CO_2 injection on the mechanical stability of faults in the Volve Field and risk of seal failure of the caprock.

Results

Based on petrophysical analysis and core testing results from exploration wells 15/9-19 A and 15/9-19 BT2 at Volve Field, we identified three injection intervals within the Hugin Formation. These intervals have an average porosity of 23% and permeability ranging from 100 mD to over 1000 mD (Fig. 5).

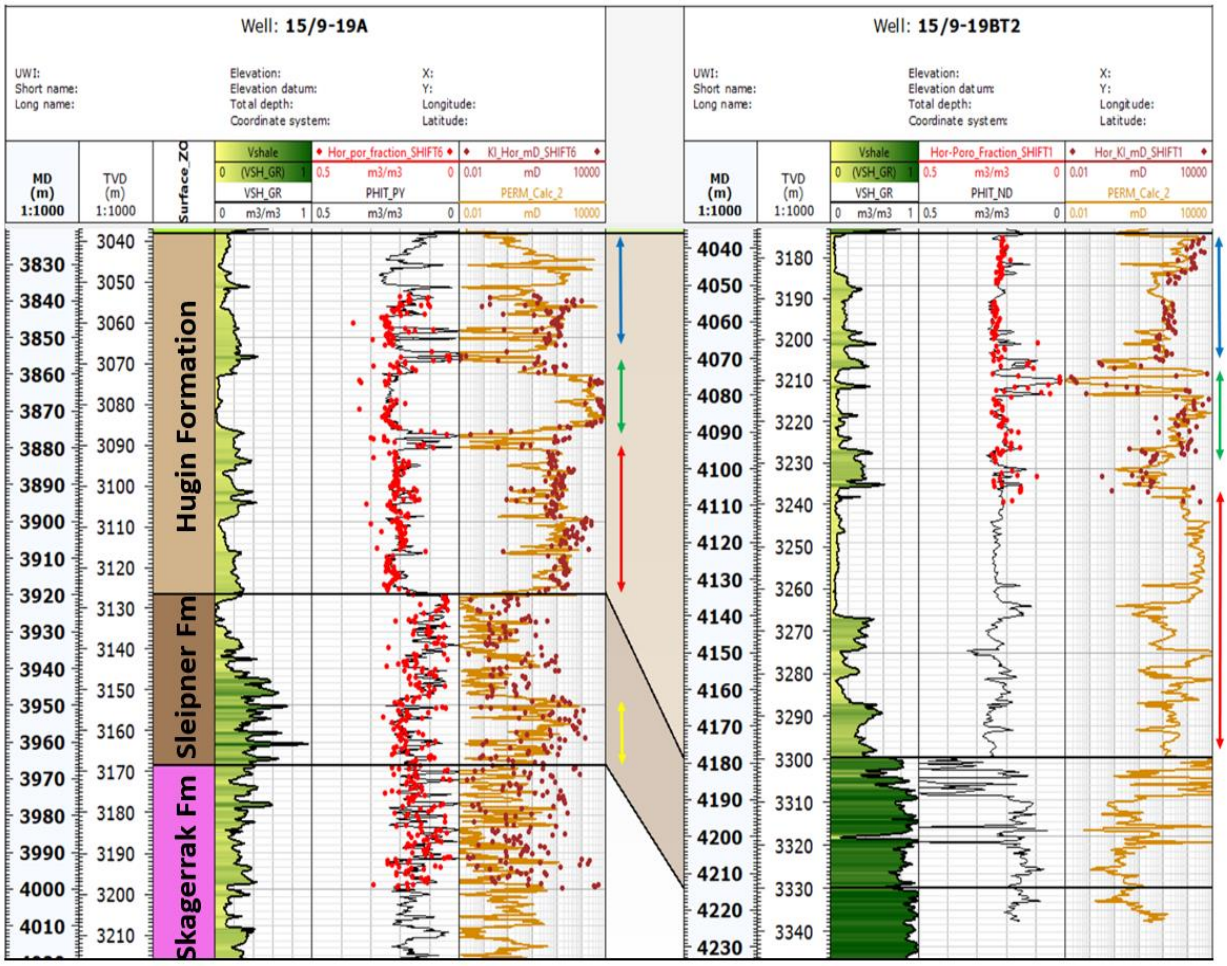

Fig. 5. Porosity and permeability chart for discovery wells 15/9-19 A and 15/9-19 BT2 in Triassic-Jurassic reservoir interval. Continuous lines indicate log-derived profiles, dots display core-testing data. Suitable injection intervals in the Hugin Formation are indicated by the blue, green, and red arrows, and in the Sleipner Formation – by the yellow arrows.

Using 1D MEM modeling at well 15/9-19 A, we estimated the initial pore pressure profile and the magnitudes of total principal stresses prior to the start of oil production at the Volve Field in 2007. The initial pore pressure gradient in the sedimentary successions at Volve Field was predominantly hydrostatic (~10 MPa/km) but displayed overpressure in the Draupne Shale interval, with a pressure gradient reaching up to 12.3 MPa/km. In the Hugin Formation, the estimated average in-situ principal stress gradients are as follows: the vertical stress gradient (S_V) was 22.7 MPa/km, SH_{max} was 17.52 MPa/km, and Sh_{min} was 16.85 MPa/km. These values indicate a dominant normal faulting stress regime.

Our fault seal analysis shows that most faults bounding the domal structure at the Volve Field exhibit relatively high SGR values, ranging from 0.3 to 0.7, due to their juxtaposition with the Draupne Shale (Fig. 6). These high SGR values correspond to potential CO_2 column heights ranging from 125 m to over 200 m. However, two locations along the main bounding faults exhibit low SGR values of less than 0.2, where the Hugin sands were self-juxtaposed. These areas could serve as potential leakage points, reducing the ability to support a thick CO_2 column. In contrast, leakage through intra-block faults is expected. With SGR values below 0.2, these faults are only capable of retaining CO_2 columns of approximately 20 to 25 m.

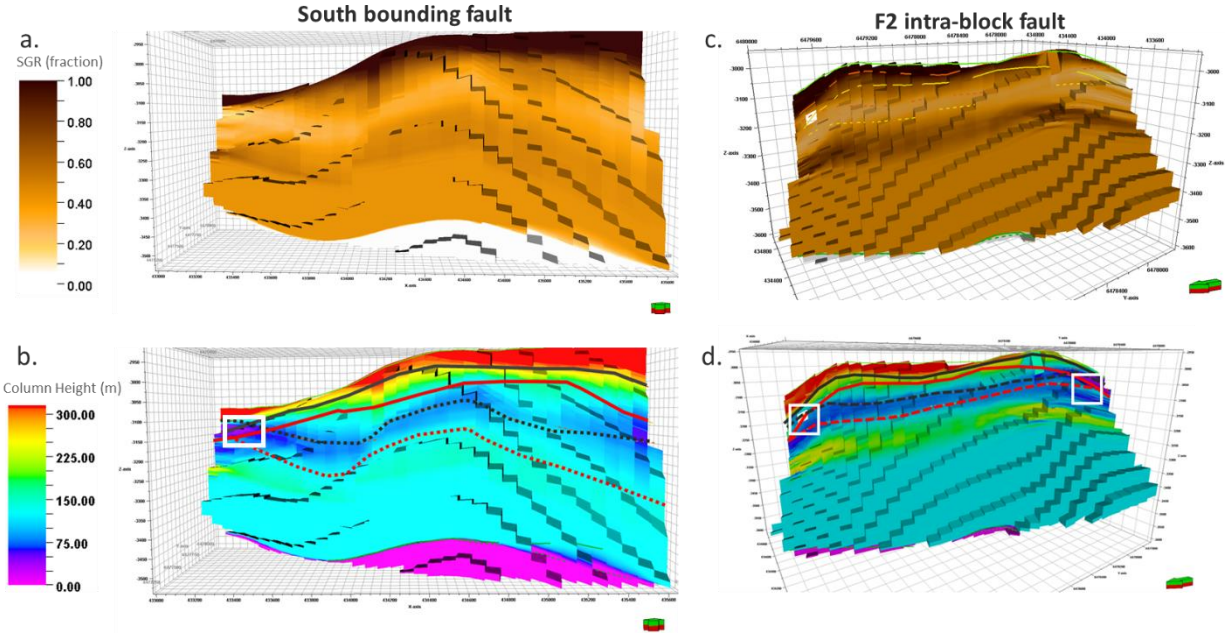

Fig. 6. SGR and predicted CO_2 column height for the NW-SE southern bounding fault (a-b) and for the NE-SW intra-block fault F2 inside the targeted domal structure (c-d). See red and orange arrows in Fig. 4a for the faults' locations, respectively. The predicted maximum CO_2 column height along the Southern bounding fault within the Hugin Reservoir is 125 m to more than 200 m. However, in the area of sand-to-sand juxtaposition (white polygons), the value drop to as low as 25 m. The lowest CO_2 column height along the F2 fault in the Hugin Reservoir is ~20-25 m in sand-to-sand juxtaposition areas (white polygons), allowing lateral fluid migration. The black and red lines represent the top and base of the Hugin Formation, respectively. Solid lines indicate the footwall, while dotted lines represent the hanging wall.

The Monte Carlo simulations using the discussed storage parameters allowed us to estimate the total CO_2 storage capacity at the injection target to range from 2.3 Mt (P90) to 6.9 Mt (P10), with a P50 value of 4.2 Mt.

The dynamic CO_2 injection simulations were carried out using several scenarios with varying maximum group injection rates over an expected injection period of 40 years (Fig. 7). In Scenario 1, with a maximum injection rate of 928.28 t/d, the maximum BHP was reached within 3 years, after which the injection rate declined and the cumulative injection volume plateaued within 21 years. In subsequent scenarios, where the maximum injection rates were reduced, the time to reach the plateau was extended. In Scenario 3, with a maximum injection rate of 185.76 t/d, the maximum BHP was reached after 28 years, and the maximum injection volume was achieved after more than 35 years of injection.

In all injection scenarios, the pressure increase due to CO_2 injection in the reservoir interval ranges between 8 MPa to 18 MPa (Fig. 7b, 9a) and the maximum CO_2 injection cumulative is around 2.1 Mt (Fig. 7a).

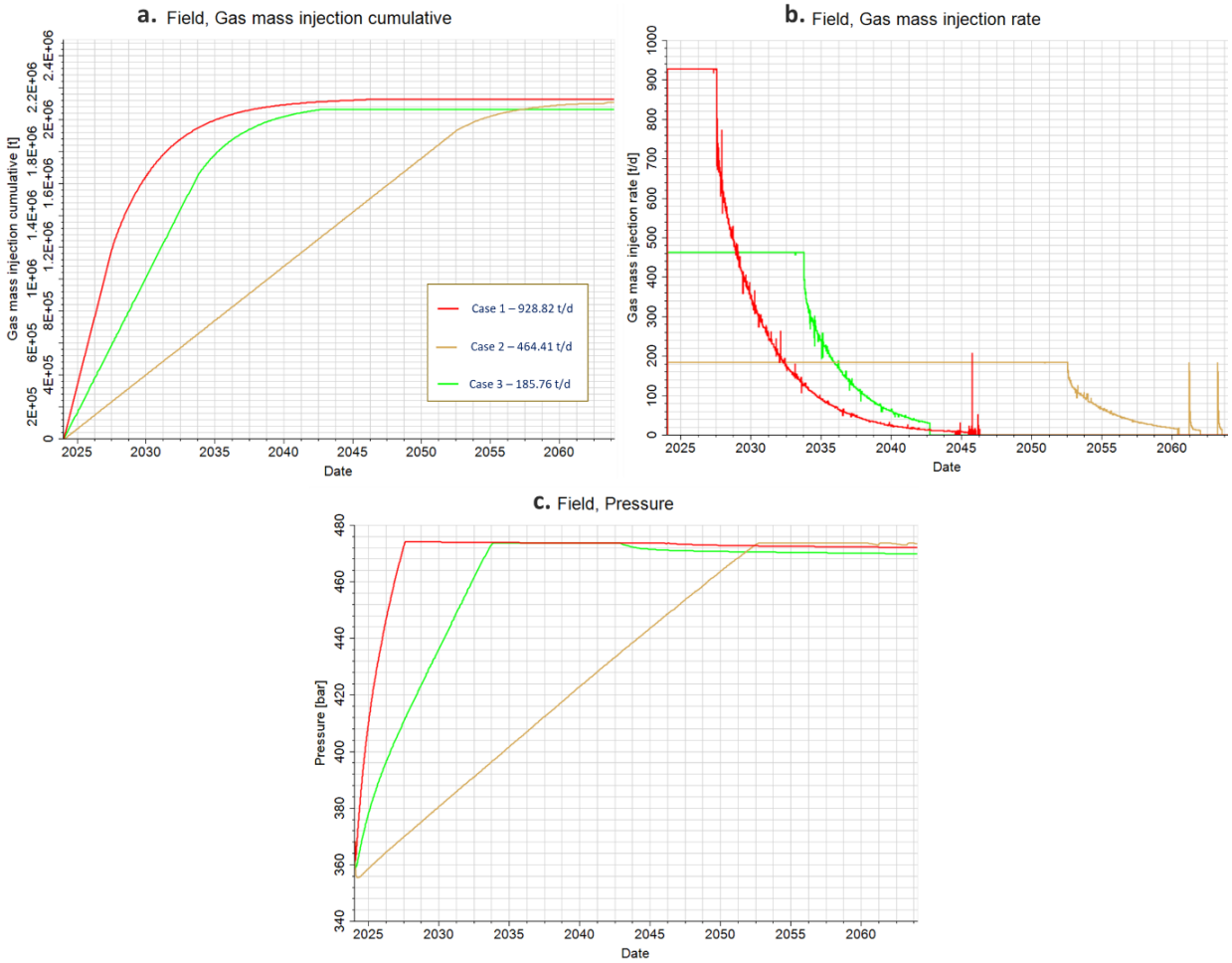

Fig. 7. The plot of CO_2 injection rate, reservoir pressure, and cumulative injection over time of different injection scenarios.

We also studied the time-step residual oil movement and CO_2 plume behaviors based on the result of the reservoir simulation using scenario 3 (Fig. 8). According to scenario 3, the remaining oil in the reservoir was mobilized towards the crest of the Volve Field anticline, creating an oil pool with an oil saturation (S_{oil}) of around 0.7 after 40 years of CO_2 injection. The cumulative saturation of the remaining oil and injected CO_2 ranges between 0.2 and 0.85 with oil concentration lower at the edges of the targeted structure in the Hugin reservoir (Fig. 8a). Plume of high concentration CO_2 dissolved in brine and oil concentrates around the 8 injection wells migrating through leaking faults toward the central part of the dome (Fig. 8b). Injected CO_2 in oil occupies mostly the southern and southeastern part of the structure (Fig. 8c).

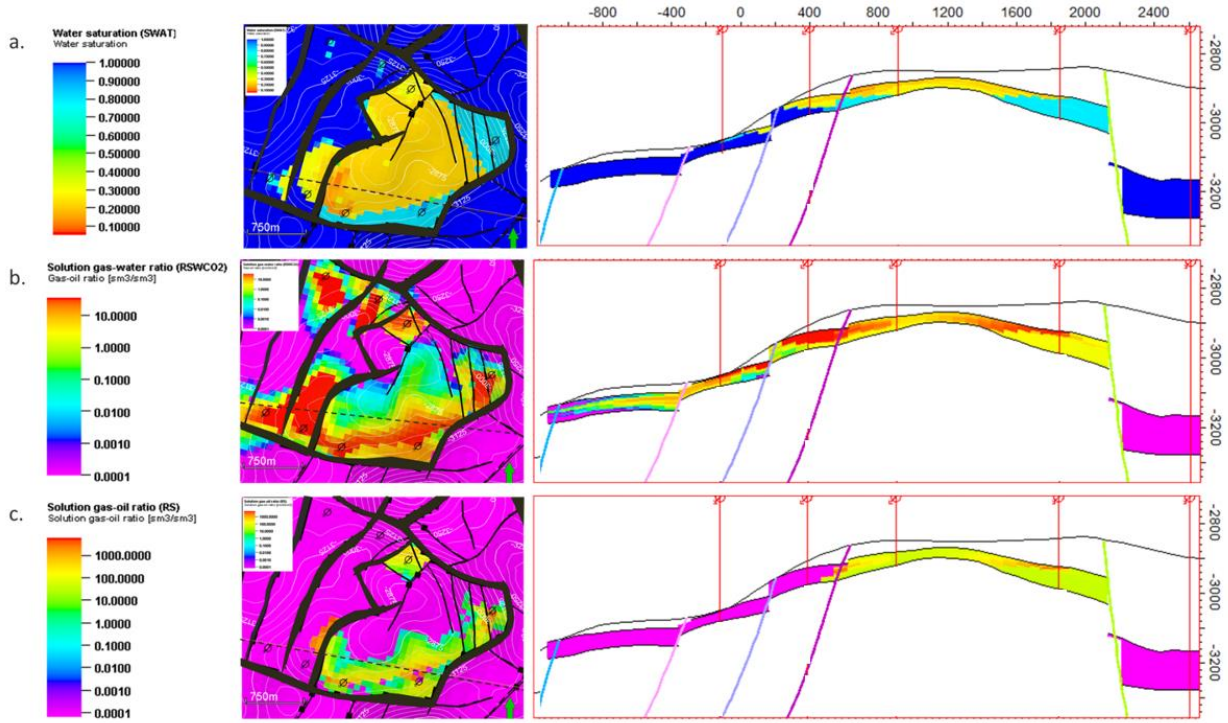

Fig. 8. Map of the top Hugin Formation and the ENE-WSW cross-section displaying predicted fluid saturations in the reservoir after 40 years of injection using scenario 3: (a) Water saturation Sw, other fluids (1-Sw) are cumulative CO_2 and remaining oil; (b) CO_2 dissolved in brine. Two limited leakage points are observed through the western tip of the Southern bounding fault and through the Northern bounding fault; (c) CO_2 dissolved in oil. High saturation of CO_2 dissolved in oil is observed at the edges of the depleted oil reservoir.

Injection wells located along the northern border of the domal structure penetrate the Hugin reservoir at relatively greater depth >3000 m), if compared to injection wells along the southern border, 3 of which penetrate the Hugin Reservoir at depth < 3000 m (Fig. 8). Higher pressure in relatively deeper reservoir interval reduces the injection wells performance, resulting in lower CO_2 volume accumulated along the northern border of the structure (Fig. 8b).

The numerically estimated low CO_2 injection cumulative volume of 2.1 Mt after 40 years of injection in the Hugin sandstone (Fig. 7c) is explained by fast pressure buildup in a relatively thin

(13-30 m) reservoir, which reaches the BHP limit after only a few years in scenario 1 to 28 years of continuous injection in scenario 3 (Fig. 7b). As a result, the injection performance drops, thus limiting the CO_2 cumulative volume.

A 3D one-way coupled geomechanical simulation was conducted using the result of scenario 3 reservoir simulation. The geomechanical modeling results suggest that reservoir pressurization due to CO_2 injection results in the increase of the magnitude of the total horizontal stresses and potential faults shear slip reactivation (Fig 9). The NW-SE bounding faults optimally oriented at about 10-20° to SH_{max} are reactivated within the reservoir interval with a maximum shear displacement of 0.0637 m. A few SW-NE intra-domal faults are also reactivated, probably because of the reservoir pressure buildup.

The effective minimum horizontal stress within both the injection interval of the Hugin Formation and the seal interval of the Draupne Formation remains positive with a minimum value of 6.42 MPa, which indicates low risk of hydraulic fracturing and CO_2 leakage through the caprock. However, additional increase of the reservoir pressure by 6.5 MPa in the critical areas may result in hydraulic fracturing.

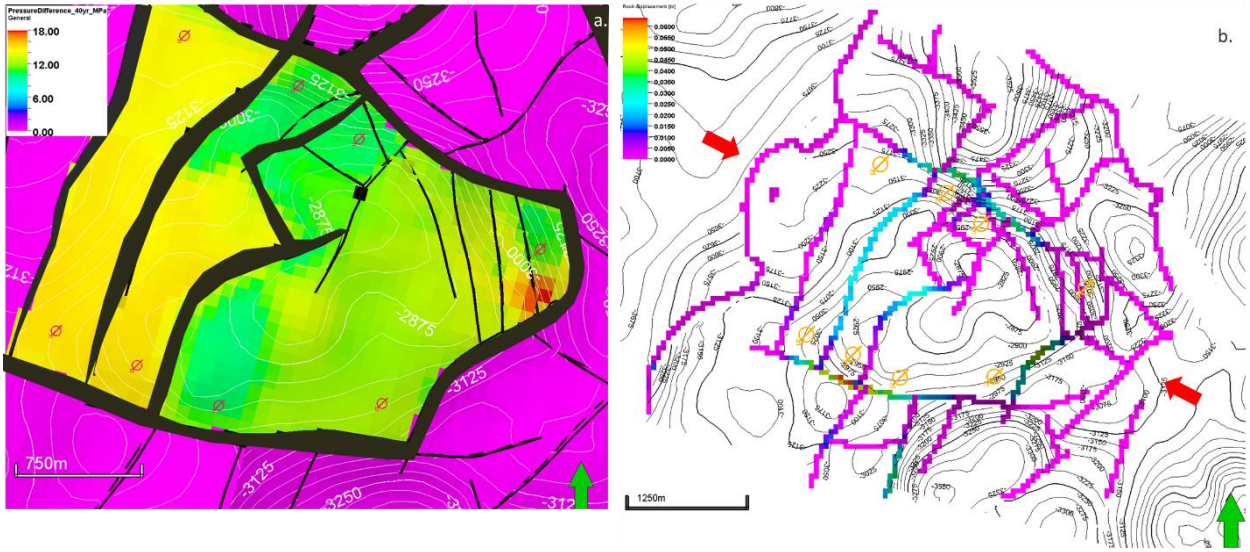

Fig. 9. (a) The increase in reservoir pressure (ΔPp) within the Hugin Formation reservoir block after 40 years of injection in scenario 3. (b) The amount of shear displacement along the reactivated faults within the Hugin Formation after 40 years of CO_2 injection (scenario 3). The maximum displacement is observed in the optimally oriented NW-SE faults at 10-20º to SH_{max}. The NW-SE block-bounding faults experience the greater shear displacement compared to the NE-SW intra-block faults. Red arrows indicate the orientation of SH_{max} at N115º while yellow circles depict the location of the simulated injection wells.

Conclusions

The petrophysical analysis of the Hugin Formation at the Volve Field revealed three suitable injection intervals with excellent porosity and permeability. The 1D MEM modeling results at well 15/9-19 A indicated initial (before production) hydrostatic pore pressure in the Hugin Formation

close to hydrostatic (11.8 MPa/km) and overpressure in the overlying Draupne Shale (12.3 MPa/km). Estimated initial magnitudes of total principal stresses correspond to normal faulting stress regime, with S_V, SH_{max}, and Sh_{min} of 22.7 MPa/km, 17.52 MPa/km, and 16.85 MPa/km, respectively. The estimated critical BHP for CO_2 injection is 47.4 MPa, to ensure Draupne Seal integrity and prevent fracturing.

Analysis of the main faults bounding the domal structure at Volve Field showed relatively high Shale Gouge Ratio (SGR) values, ranging from 0.3 to 0.7, indicating that these faults can support CO_2 columns at the reservoir interval ranging from 125 m to greater than 200 m, making leakage through these faults unlikely. However, intra-block faults with lower SGR values (<0.2) allowing CO_2 across-fault migration to the center of the domal structure. As most of the faults do not penetrate the sealing units of the thick Draupne Formation, the risk of upward CO_2 leakage is relatively low.

CO_2 injection simulations conducted under various scenarios revealed that in Scenario 1, with a maximum injection rate of 928.28 t/d, the maximum BHP was reached within three years, and the cumulative injection volume plateaued after 21 years. In Scenario 3, with a lower injection rate of 185.76 t/d, the maximum BHP was reached after 28 years, and the full injection volume was achieved after more than 35 years. Pore pressure increase in the reservoir after 40 years of injection (scenario 3) average around 10.6 MPa.

We conducted two separate CO_2 storage capacity estimates: one using a Monte Carlo simulation based on static reservoir properties obtained from core petrophysical measurements and literature studies, and the other based on dynamic reservoir simulation results. The Monte Carlo simulation estimated a P50 storage capacity of 4.2 Mt, while the dynamic reservoir simulation estimated a capacity of 2.1 Mt after 40 years of injection at a rate of 185.76 t/d in scenario 3. The estimated low CO_2 injection cumulative volume of 2.1 Mt after 40 years of injection (dynamic simulation) in the Hugin Sandstone is explained by a fast pressure buildup in a relatively thin (13-30 m) of the reservoir, which reaches the BHP limit after a few years to 28 years of continuous injection, depending on the injection rate. As a result, the injection performance drops, thus limiting the CO_2 cumulative volume.

The next step of study aims at simulating CO_2 injection into the wet sand of the Sleipner Formation, which, although heterogeneous, has a greater thickness (40-67 m) and intervals of good porosity (up to 20%) and permeability (10-100 mD) in the lower interval. CO_2 injection in the Sleipner reservoir will result in slower reservoir pressure buildup and higher injectivity, suggesting the Sleipner Formation might represent a better target, which would be able to maintain injectivity and represent an economically more viable alternative to the Hugin Formation.

Finally, a 3D one-way coupled geomechanical simulation based on Scenario 3 showed that pressurization from CO_2 injection caused an increase in total horizontal stresses after 40 years of injection. Optimally oriented faults show fault shear slip reactivation with maximum shear displacement of 0.0637 m at the reservoir interval. Despite these changes, the minimum effective horizontal stress within both the injection reservoir and the seal layers remained positive, indicating low risk of hydraulic fracturing and CO_2 leakage. The minimum values of the minimum effective horizontal stress is 6.42 MPa, so an additional increase of reservoir pressure by 6.5 MPa should be avoided.

Acknowledgements

The authors would like to thank Equinor for providing access to open-source data from the Volve Field dataset. We also express our gratitude to SLB for donating the consolidated Petrel-Intersect-Visage-Techlog license, and to Rose Subsurface Assessment for donating the RoseRA Prospect and Risk Analysis Software to the University of Alberta. Special thanks to Pieter Pestman, Peter Carraghar, Phil Conway, Jim Gouveia, David Cook, and Juliet Irvin from Rose Subsurface Assessment for their valuable knowledge and ongoing technical support, which significantly enhanced the methods used in this research. This work was funded by the Natural Sciences and Engineering Research Council of Canada (NSERC) through grants RGPIN 2019-04397 and DGECR 2019-00186.

References

1. Bachu, S. (2003). Screening and ranking of sedimentary basins for sequestration of CO_2 in geological media in response to climate change. Environmental Geology, 44(3), 277–289. https://doi.org/10.1007/s00254-003-0762-9.
2. Barclay, T. H., & Mishra, S. (2016). New correlations for CO_2-oil solubility and viscosity reduction for light oils. Journal of Petroleum Exploration and Production Technology, 6(4), 815–823. https://doi.org/10.1007/s13202-016-0233-y.
3. Burnside, N. M., & Naylor, M. (2014). Review and implications of relative permeability of CO_2/brine systems and residual trapping of CO_2. International Journal of Greenhouse Gas Control, 23, 1–11. https://doi.org/10.1016/j.ijggc.2014.01.013
4. Callas, C., Saltzer, S. D., Davis, J. S., Hashemi, S. S., Kovscek, A. R., Okoroafor, E. R., Wen, G., Zoback, M. D., & Benson, S. M. (2022). Criteria and workflow for selecting depleted hydrocarbon reservoirs for carbon storage. Applied Energy, 324, 119668. https://doi.org/10.1016/j.apenergy.2022.119668.
5. Eaton, B. A. (1975). The equation for geopressure prediction from well logs. Fall Meeting of the Society of Petroleum Engineers of AIME.
6. Equinor. (2018). Volve Field Dataset. Retrieved from https://www.equinor.com/energy/volve-datasharing.
7. Goodman, A., Sanguinito, S., Levine, J.S. (2016). Prospective CO_2 saline resource estimation methodology: refinement of existing US-DOE-NETL methods based on data availability. Int. J. Greenhouse Gas Control 54, 242–249.
8. Grollimund, B., Zoback, M. D., Wiprut, D. J., & Arnesen, L. (2001). Stress orientation, pore pressure, and least principal stress in the Norwegian sector of the North Sea. Petroleum Geoscience, 7(2), 173–180.
9. Halland, E. K., Gjeldvik, I. T., Johansen, W. T., Magnus, C., Meling, I. M., Pedersen, S., Riis, F., Solbakk, T., & Tappel, I. (2024). CO_2 storage atlas of the Norwegian North Sea. The Norwegian Petroleum Directorate.
10. Heidbach, O., Rajabi, M., Cui, X., Fuchs, K., Müller, B., Reinecker, J., Reiter, M., Tingay, F., Wenzel, F., Xie, M., Ziegler, M.-L., & Zoback, M. D. (2018). The World Stress Map database release 2016: Crustal stress pattern across scales. Tectonophysics, 744, 484–498. https://doi.org/10.1016/j.tecto.2018.07.007.
11. Hillis, R. R., & Nelson, E. J. (2005). In-situ stresses in the North Sea and their applications: Petroleum geomechanics from exploration to development. Petroleum Geology: Northwest Europe and Global Perspectives. Proceedings of the 6th Petroleum Geology Conference, 6, 551–564.
12. IEA-GHG, 2009. Development of Storage Coefficients for CO_2 Storage in Deep Saline Formations: IEA Green House Gas R&D Programme (IEA-GHG), Report No. 2009/13. pp. 118.
13. Karlo, J. F., Van Buchem, S. P., Moen, J. D., & Milroy, K. (2014). Triassic-age salt tectonics of the Central North Sea. Interpretation, 2(1), SM19–SM28. https://doi.org/10.1190/INT-2014-0032.1.
14. Mao, S., Zhang, D., Li, Y., & Liu, N. (2013). An improved model for calculating CO_2 solubility in aqueous NaCl solutions and its application to CO_2–H_2O–NaCl fluid inclusions. Chemical Geology, 347, 43–58. https://doi.org/10.1016/j.chemgeo.2013.03.010.
15. Marín, D. L. R., Cedeño, A., Rojo, L., Escalona, A., Dyskeland, J., & Skarstein, G. (2022). Importance of evaporitic successions in geothermal energy and near-field exploration in the Norwegian North Sea. EAGE Conference Proceedings.
16. Norwegian Offshore Directorate. (2025). Volve. Retrieved from https://www.norskpetroleum.no/en/facts/field/volve.

17. Ravasi, M., Vasconcelos, I., Curtis, A., & Kristi, A. (2015). Vector-acoustic reverse time migration of Volve ocean-bottom cable data set without up/down decomposed wavefields. Geophysics, 80(4), S137–S150.
18. Sanguinito, S., Singh, H., Myshakin, E. M., Goodman, A. L., Dilmore, R. M., Grant, T. C., et al. (2020). Methodology for estimating the prospective CO_2 storage resource of residual oil zones at the national and regional scale. International Journal of Greenhouse Gas Control, 96, 103006. https://doi.org/10.1016/j.ijggc.2020.103006.
19. Szydlik, T. J., Way, S., Smith, P., Aamodt, L., & Friedrich, C. (2006). 3D PP/PS prestack depth migration on the Volve Field. 68th EAGE Conference and Exhibition Incorporating SPE EUROPEC 2006. https://doi.org/10.3997/2214-4609.201402177.
20. Thiercelin, M. J., & Plumb, R. A. (1994). Core-based prediction of lithologic stress contrasts in East Texas formations. SPE Formation Evaluation, 9(3), 251–258. https://doi.org/10.2118/21847-PA.
21. Weijermars, R. (2024). Fast production and water-breakthrough analysis methods demonstrated using Volve Field data. Petroleum Research, 9, 327–346. https://doi.org/10.1016/j.ptlrs.2024.03.001
22. Yielding, G., Bretan, P., & Freeman, B. (2010). Fault seal calibration: A brief review. In S. J. Jolley, Q. J. Fisher, R. B. Ainsworth, P. J. Vrolijk, & S. Delise (Eds.), Reservoir Compartmentalization, 347. Geological Society of London Special Publications, 243–255.
23. Zoback, M. D. (2010). Reservoir Geomechanics. Cambridge University Press.